Electrochemical Fabrication of Nanostructures

2

R. Abdel-Karim

Contents

Abstract

Electrodeposition is a unique technique in which a variety of materials can be produced including metals, ceramics, and polymers. In the current chapter, the advantages of electrochemical deposition techniques in fabricating various nanomaterials with superior properties compared with conventional materials will be highlighted. The properties of various nanostructured coatings produced by electrodeposition are discussed. Some models describing nucleation and growth mechanism are presented. Finally, the importance of some nanocrystalline electrodeposits in many industrial applications as well as their potential role in the

R. Abdel-Karim (✉)
Department of Metallurgy, Faculty of Engineering-Cairo University, Giza, Egypt
e-mail: randaabdelkarim@gmail.com

M. Aliofkhazraei, A.S.H. Makhlouf (eds.), *Handbook of Nanoelectrochemistry*,
DOI 10.1007/978-3-319-15266-0_18

planned future technologies is emphasized. The potential of highly ordered nanomaterials for future technological applications includes the field of various nanophotonic, catalytic, microfluidic, and sensing devices, as well as functional electrodes and magnetic recording media. Another application is template-assisted electrodepositiion employing a variety of nanoporous membranes and films such as nanoporous alumina membranes used for the synthesis of high-density, ordered arrays of nanodots, nanotubes, and nanowires.

Keywords

Electrocrystallization • Nucleation and growth • Metals • Alloys • Nanocomposites • Nanorods • Nanowires • Nanoporous membranes

Introduction

Nanocrystalline materials with grain size of less than 100 nm are a new and novel class of advanced materials, which are intensively applied in the scientific and business communities. Since their introduction in the early 1980s [1], intensive scientific activity in the areas of production, microstructural characterization, and property determination of these materials has resulted in the development of a number of manufacturing techniques capable of producing various materials with superior properties over conventional materials [2]. Consequently, several industrial applications and hence new market opportunities have emerged from this field and are continuing to increase in numbers. Most current efforts on large-scale production of nanostructured materials are concerned with consolidating nanocrystalline precursor powders produced by techniques such as gas condensation, ball milling, or spray conversion. Film deposition techniques such as physical and chemical vapor deposition, sol–gel techniques, etc. are also under intensive research activities.

A thin coating (thickness up to -100 μm) electroplated onto on a substrate to modify specific surface properties is probably the most widely known application of electrodeposition technologies. However, it should be noted that there are several other processes (e.g., brush plating, electrowinning, and electroforming) which can be used to produce nanocrystalline materials as thick coatings (several mm or cm thick) or in freestanding forms such as sheet, foil, tubes, wire, mesh, plate, and foam [3]. Table 1 summarizes the nano products obtained from each process.

The production of nanomaterials requires a deposition process on the atomic level and extreme control over the deposition. The obvious advantages of this century-old process of electrodeposition are as follows:

(a) High production rate and low cost
(b) Free from porosity and high purity
(c) Industrial applicability

Table 1 Different techniques for production of nanomaterials

Nanoproduct	Production techniques
Powders	Gas condensation, ball milling, or spray conversion
Thin coatings	Physical and chemical vapor deposition, sol–gel techniques, electrodepsoition
Thick coatings Freestanding forms such as sheet, foil, tubes, wire, mesh, plate and foam	Brush plating, electrowinning and electroforming

(d) Ability to overcome shape limitations or allow the production of freestanding parts with complex shapes
(e) Coating on widely differing substrates
(f) Ability to control structural features with sizes ranging from nm to μm
(g) Control of the alloy composition and the ability to produce alloys with composition unattainable by other methods
(h) The possibility of forming of simple low-cost multilayers in many different systems
(i) No requirements of postdeposition treatment [3]

Electroplating is a technologically feasible and economically superior technology for the production of nanostructured pure metals and alloys as well as nanocomposites [2]. Electrochemical deposition of polycrystalline metals and alloys exhibits several types of growth forms such as layers, blocks, ridges, pyramids, spiral growth, dendrites, powders, and whiskers [4]. Mohanty [5] has demonstrated the electrodeposition of various nanostructure materials, such as nanoparticles, nanowires of Au, Pt, Ni Co, Fe, Ag, etc., for example, the synthesis of nanocrystalline pure metals e.g., Ni [6], Co, and Cu [7], binary alloys e.g., Ni-P [8], Ni-Fe [9], Zn-Ni [10], and Co-W [11], and ternary alloys e.g., Ni-Fe-Cr [12] and Ni-Mo-Fe [13]. Even multilayered structures or compositionally modulated alloys (e.g., Cu-Pb and Ni-P, metal matrix composites e.g., Ni-Si C, and ceramics e.g., ZrO_2 have been successfully produced by electrodeposition techniques [14].

Theory of Electrodeposition

The mechanism of electrodeposition is similar to the crystal growth of conventional metals and is developed in two steps:

(i) Formation of nuclei covering electrode with few atomic layers of metal
(ii) Growth of deposits

Formation of nuclei requires high voltage although once formed, nuclei will grow fast at low voltage. The atoms (adatoms), which are formed during the

electroplating on the crystal plane quickly, occupy suitable sites, such as kink sites where atoms interact with three neighbors or edge sites (two neighbors) and sometimes occupy terrace sites (one neighbor).

The growth takes place through the following steps:

(a) Mass transport in solution by diffusion of ions to the surface of cathode
(b) Electron transfer to form an adatom (a mobile or absorbed atom)
(c) Diffusion of adsorbed atoms across the surface to kink sites [15]

Nucleation

The nucleation and growth processes taking place during electrodeposition of metal coatings are similar to that occurring during any conventional crystallization process. They differ in that, in the case of electrocrystallization, the metal atoms required for nucleation must first be present. The hydrated metal ions transfer across the metal-solution interface and then neutralize at the cathode surface, forming the local crystal nuclei. On the other hand, in the case of crystallization from molten metal, the uncharged metal atoms collect to form crystal nuclei, which then grow spontaneously, as soon as a critical size is reached [16].

Homogeneous Nucleation

When the temperature falls below the melting point, the molten metal is cooled, and the first crystal nuclei are formed. The process results in thermal energy change, as the state changes from liquid to solid. The so-called Gibbs free energy (G) of all elements is then equal to zero. However, this is true only for each element in a defined state (liquid, solid, gaseous) and at a given temperature. As metal atoms solidify, the kinetic energy, ΔGv, is designated with a minus sign due to contraction in volume.

On the other hand, as a solid nucleus is formed, an interface must be formed between this nucleus and the surrounding melt. For this, some surface work (ΔG°) is required, which therefore is positive. The surface energy γ between the crystal surface and the deposited layer depends on the type of metal as well as the surface area of the nucleus. The total change in Gibbs free energy, ΔG, for the formation of a spherical nucleus of radius r, volume $V_K = (4/3)\,\pi r^3$, and surface area $= 4\,\pi r^2$ is the sum of volume energy and surface energy, ΔGv and ΔG°

$$\Delta G = \Delta Gv + \Delta G^{\circ} = -\left(4/3\right)\pi r^3 \cdot \Delta Gv + 4\pi r^2 \gamma \tag{1}$$

The crystal nuclei with $r > r^*$ are thermodynamically stable and will probably continue growing. On the other hand, if $r < r^*$, the nucleus is not thermodynamically stable and is likely to contract in size, and it dissolves. Further growth of such small nuclei is accompanied by an increase in Gibbs free energy [16].

Heterogeneous Nucleation

In this case, nucleation and growth initiates at the mold wall or perhaps around solid impurities in the melt. These are known as initiation sites and act as active centers, reducing activation energy need for formation of nuclei of greater than the critical size. The change in free energy ΔG^{**} is not only a function of the radius of the nucleus but also of the wetting angle θ.

If $\theta = 0$, a complete wetting of the wall surface by the nascent crystal nucleus occurs and $\Delta G^{**} = 0$, which corresponds to spontaneous crystallization from the melt, without any activation energy barrier.

If $\theta = 180$, there is no wetting of the container wall by the growing nuclei, and the relationship $\Delta G^{**} = \Delta G^{*}$ is obtained. This condition represents a homogeneous nucleation and requires the highest energy of formation of a nucleus. The formation of nuclei of at least the critical size can result when the metal ions pass directly to the cathode surface at nucleation sites, where this is energetically favored. Another option is that they pass through sites which are energetically less favorable. In the latter case, lateral movement of adsorbed atoms across the surface is necessary to form nuclei of the critical size [15].

As adatoms reach the cathode, the hydrated metal ions lose a part of their hydration sheath and thus retain a partial charge. In this especially low-energy state, they diffuse across the cathode surface to the nearest growth site. Depending on the location and state of the resulting crystal nucleus, four different types of site are recognized. These are zero-dimensional sites and one-, two-, and three-dimensional sites (edge, plane, or corner sites, respectively).

1. Zero-dimensional nuclei:
   This represents the deposition of individual adatoms onto an active site at the cathode surface. Formation of such nuclei requires the smallest of all energies of nucleation.
2. One-dimensional nuclei:
   When a series of adatoms accumulate along the edge of a monoatomic step at the cathode surface, the nucleation energy required for this is somewhat higher than in case 1.
3. Two-dimensional nuclei:
   This situation illustrates a planar agglomeration of adatoms, the orientation of which will often depend on that of the underlying substrate. This effect is known as “epitaxy,” where the lattice structure of the deposit is either identical to that of the cathode or very similar.
4. Three-dimensional nuclei:
   The lattice structure of the deposit differs from that of the cathode. In practice, the conditions for forming such nuclei are extremely complex. The interaction between a crystal nucleus and the substrate depends on their lattice structures. This is in the case of a totally smooth and featureless substrate.

The nucleation may exhibit epitaxial behavior if the lattice structures of substrate and deposited metal are identical or similar. In case of three-dimensional

nucleation, lattice defects such as edges, corners, and steps are presented at the cathode surface. The nucleation energy for three-dimensional nuclei is always larger than that for two-, one-, or zero-dimensional types [15].

The rate of nucleation dN_k/dt is presented as follows:

$$\frac{dN_K}{dt} = a_K \cdot \exp\left(-\frac{\overline{\Delta G}^*}{RT}\right) \tag{2}$$

where a_K is a constant of the system.

According to the following equation, the critical nucleus size decreases as the crystallization overvoltage η_k, increases:

$$\eta_K = \frac{2\gamma V}{zF\,\overline{r}^*} = \frac{RT}{zF}\ln\frac{c_{ad}}{c^\circ_{ad}} \tag{3}$$

where

V is the molar volume of a crystal nucleus of critical size.
z is the number of electrons transferred.
c_{ad} is the concentration of adatoms at a growth site.
c°_{ad} is the concentration of adatoms in the equilibrium state.

Increasing the concentration of adatoms will lead to increase in both the crystallization overvoltage and the rate of nucleation [17, 18].

Growth of Nuclei

The electrodeposit formation takes place by the following steps:

- Ions of the solvent move through the cathode by diffusion, migration, and convection.
- There is an electron transfer between the cathode and the ions.
- There is partial or total loss of the solvation spheres and adatom formation.
- The adatoms are absorbed by the surface and spread till they find suitable sites.
- There is cluster formation.
- There is crystallographic development of the crystal grain [15].

According to the model of Kossel and Stansky, the crystal growth occurs through competition between vertical growth, depending on two-dimensional nucleation rate, and horizontal growth, depending on the rate of the repeatable step [19]. The Kossel-Stansky model assumed that the strength of binding of an atom to the surface depends on its number of nearest neighbors. They applied this to a simple cubic crystal, which is also known as a Kossel crystal. According to this theory, metal atoms are preferentially deposited at sites on the cathode surface where their incorporation in the lattice releases the most energy. On this basis, preferential growth of

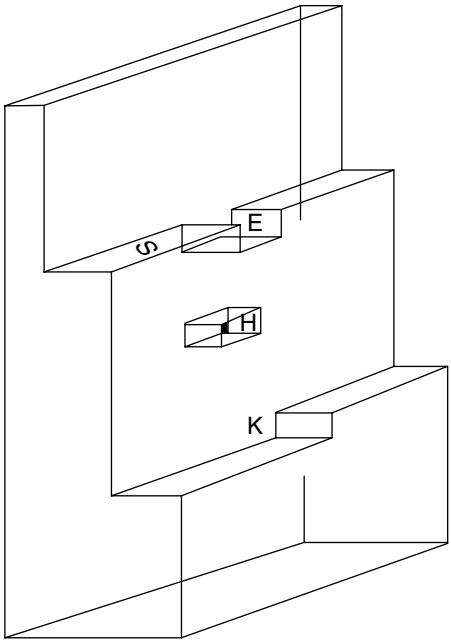

Fig. 1 Different growth sites at a substrate. E = corner; H = recess; K = edge; S = step [17]

nuclei is expected at the locations such as edges, corners, steps, and kinks. Metal atoms at the surface of the lattice have unbound valence bonds that exert an effect on their immediate environment which is most pronounced at the topographic features listed above, where it is said that individual atoms are more exposed. That's why preferential metal deposition occurs at these locations, where the free energy required is at a minimum. These locations are also known as semicrystalline. At these topographic features, the highest current density is observed, which motivates the crystal growth rate [16]. According to the Terrace-Ledge-Kink (TLK) model, metal atoms are preferentially deposited at edges, corners, steps, and kinks (Fig. 1) where overall the free energy needed is minimum [17].

Incoming adatoms build up, either directly or after lateral diffusion, at the defect sites presented on the cathode surface. The stability of growing nuclei formed at these locations is determined by the local lattice energy required to incorporate more atoms into the metal matrix at the cathode. Later on, it was realized that crystal growth can occur by means of the rotational movement of a growing spiral at a screw dislocation [15].

Modes of Thin-Film Growth

These are monolayer overgrowth, nuclear growth, and the growth mode that has both features of the former two. The monolayer overgrowth mode is described in Fig. 2b and is also called Frank-van der Merwe mode (FvdM mode).

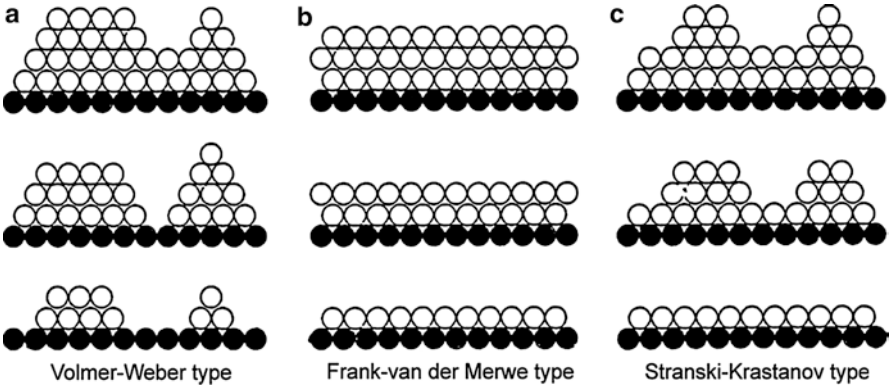

Fig. 2 Different modes of thin-film growth; (**a**) Volmer-Weber (V-W) type, (**b**) Frank-van der Merwe (F-M) type, and (**c**) Stranski-Krastanov (S-K) type [19]

The deposited atoms (or molecules) cover the substrate uniformly by one atom thickness, and the deposit grows layer by layer. This growth mode occurs when the substrate material and the growth material have good amicability and low surface tension [19].

Another mode is called island growth or Volmer-Weber mode (VM mode). When the desorption process is not strong, the atoms, which reach the substrate, form two-dimensional gases on it, and they condense forming a nucleus with high density. High density of nucleus leads to touch and combine each other, and they grow to an island. When it further grows, it becomes a channel state, a whole state, and finally makes a uniform thin layer as shown in Fig. 2a. The VM mode differs from FvdM mode in that VM mode does not grow layer by layer. This mode is chosen in case of high surface tension of the growth material and low amicability between the substrate materials and the growth deposit.

Stranski-Krastanov growth mode is an intermediate process consisting of both 2D layer and 3D island growth. Transition from the layer-by-layer to island-based growth occurs at a definite critical coating thickness which depends mainly on the chemical and physical properties, such as surface energies and lattice parameters, of the substrate and the coating layer [20–22].

The growth of epitaxial (homogenous or heterogeneous) layers on a single crystal surface depends critically on the interaction strength between adatoms and the substrate. In Volmer-Weber (VW) growth mode, adatom-adatom interactions are stronger than those of the adatom with the substrate material, resulting in the formation of three-dimensional adatom clusters or islands [21]. Growth of these clusters, accompanied with coarsening, will lead to rough multilayer film formation on the substrate. On the other hand, during Frank-van der Merwe (FM) growth mode, adatoms are attached preferentially to surface sites resulting in the formation of atomically fully smooth layers. This layer-by-layer growth is two dimensional leading to complete film formation before the growth of subsequent layers [22].

Markov [23] proposed an equation for the layer chemical potential per atom as

$$\mu(n) = \mu_{\infty} + \left[\varphi_a - \varphi_a^{'}(n) + \varepsilon_d(n) + \varepsilon_e(n)\right] \tag{4}$$

where μ_{∞} is the bulk chemical potential of the adsorbate material, φ_a the desorption energy of an adsorbate atom from a wetting layer of a material similar to the substrate material, $\varphi_{a'}(n)$ the desorption energy of an adsorbate atom from the substrate, $\varepsilon_d(n)$ the misfit dislocation energy per atom, and $\varepsilon_e(n)$ the homogeneous strain energy per atom. In general, the value of φ_a, $\varphi_{a'}(n)$, $\varepsilon_d(n)$, and $\varepsilon_e(n)$ is dependent in a complex way on the thickness of the growing layers and lattice misfit between the substrate and adsorbate layer.

In case of small strains, $\varepsilon_{d,e}(n) \ll \mu_{\infty}$, the criterion that determines the film growth mode depends on the chemical potential change per unit atom $\frac{d\mu}{dn}$.

- For VW growth mode, $\frac{d\mu}{dn} < 0$ (adatom cohesive force is higher than surface adhesive force)
- For FM growth mode, $\frac{d\mu}{dn} > 0$ (surface adhesive force is higher than adatom cohesive force)

SK growth can be characterized by both of these inequalities. While initial deposit growth follows a FM mechanism, i.e., positive differential μ, nontrivial amounts of strain energy accumulate in the deposited layers. At a critical thickness, this strain induces a sign reversal in the chemical potential, i.e., negative differential μ, leading to a change in the growth mode. At this point, it is energetically preferred to nucleate islands, and additional growth is favored by a VW mode [23].

Attachment of the thinner deposit to the thicker substrate causes a misfit strain "Є" at the interface given by

$$\text{Є} = (a_f - a_s)/a_s \tag{5}$$

where a_f and a_s are the deposit and substrate lattice constants, respectively.

As the wetting layer thickness is higher, the resulting strain energy increases rapidly. In order to lower the strain, island formation can take place in either a dislocated or coherent mode. In dislocated islands, strain relief results from interfacial misfit dislocations. The reduction in strain energy accommodated by forming a dislocation is generally greater than the effect of increasing surface energy associated with creation of the new clusters. The thickness of the wetting layer at which island nucleation is formed, called the critical thickness h_C, is strongly dependent on the lattice mismatch between the layer and substrate. Higher mismatch leads to smaller critical thicknesses for deposit formation [24].

Microstructures of Electrodeposits

Fischer [25] recognized five main growth morphology types for polycrystalline electrodeposits: field-oriented isolation, basis-oriented reproduction, twinning intermediate, field-oriented texture, unoriented dispersion type. This model was based on previous work of Winand [18], which is summarized in Fig. 3.

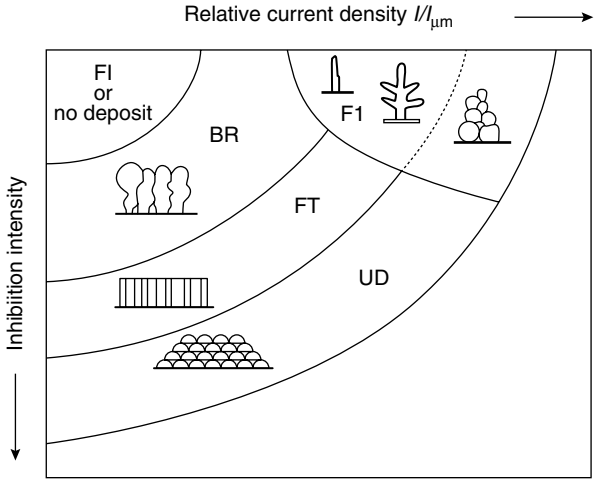

Fig. 3 Winand diagram of surface morphology depending on current density and inhibition activity [18]

(i) Field-oriented isolated crystal type (FI)
At low overvoltage (0–10 mV), a one-dimensional nucleation is observed. The nuclei grow to form individual crystallites, usually oriented in the axis of the current field. Growth occurs slowly at the side faces of these crystallites, and dendritic layers are deposited. These deposits have no useful technical properties.

(ii) Base-oriented reproduction type (BR)
At higher overvoltage of 10–100 mV, a two-dimensional nucleation occurs, and flat-faced crystallites grow. The technical properties of these deposits are interesting because they are similar to those of the underlying substrate.

(iii) Field-oriented texture type (FT)
In the range of 100–150 mV of overvoltage, single crystallites initially form. If the overvoltage increases, the crystallites become three-dimensional, which grow parallel to the electric field lines and whose bounds are crystallites.

(iv) Unoriented dispersion type (UD)
At overvoltage higher than 200 mV, small crystals are formed as a result of high rates of electrocrystallization. The result is a microstructure of very fine randomly oriented crystallites with two visible grain structures. Deposits of this type are ideal for technical applications, due to their excellent properties.

(v) Twinning transition type (Z)
This type of growth represents the transition between FT and BR type. This structure is formed when the crystallization overvoltage is large enough to allow formation of two-dimensional nuclei. Twinning may cause a reduction of the ductility of the deposited metal.

Nanoelectrodeposited Metals and Alloys and Their Properties

As indicated in Table 2, the electrodeposition technology has been used to produce a wide range of nanostructured materials, e.g., metal nanoparticles, nanowires, nanofilms, bulk NC metals, laminated composites, multilayered coatings, and nanoparticle-reinforced composite coatings. The electrodeposited nanostructured layers could be pure metals, alloys, composites, or sandwich layers.

Gold-Based Deposits

Au

A lot of intensive research was directed toward gold nanostructures, which is applied for many applications as substrates for surface-enhanced Raman scattering (SERS), super-hydrophobicity catalysis or sensors, selective solar absorbers, antireflection coatings, or diffraction gratings. The surface morphology of gold, especially the roughness, influences their functional properties. The catalytic activity of metal nanostructures is dependent on surface morphology [26].

Bossini et al. [29] studied the galvanostatic electrodepsoition of nanogold using cyanocomplex Au(I) baths with citrate additives. The structural effects of organic

Table 2 Different electrodeposited nanometerials, properties and applications [3, 26–28]

Materials	Properties and applications
Au based alloys	
Au, Au–Cu	Substrates for surface-enhanced Raman scattering (SERS) technique, super-hydrophobicity catalysis or sensors, selective solar absorbers, antireflection coatings or diffraction gratings
Pd-based alloys	
Pd, Ni–Pd	Hydrogen storage and purification, electrodes for hydrogen evolution and fuel cells
Co-based alloys	
Co, Co–W, Co–P	Good candidates for the replacement of the highly toxic hexavalent chromium in plating baths, due to their excellent mechanical and wear resistant properties. These materials have high saturation magnetization, good thermal stability and extraordinary hardness
Co–Ni–Cu	Good catalyst for hydrogen evolution
Ni-based alloys	
Ni, Ni–W, Ni–P, Ni–Mo, Ni–Co, Ni–Cu, Ni–Zn, Ni–Mg, and Ni–B	Good magnetic properties, corrosion protection, stress corrosion and Electrocatalytic activity for hydrogen evolution
Ni–Al_2O_3, Ni–SiC	Corrosion protection, wear resistance
Ni–Fe–Cr	Cracking resistance, soft magnets, catalysts

additives have been explained on the basis of competitive adsorption and cathodic reaction of the organics. In situ SERS measurements have explained the molecular aspects of grain growth inhibition and related stabilization of adatom clusters and nanocrystalline structures. The adsorption behavior of cyanide during the electrodeposition of gold has been investigated by in situ Raman spectroscopy.

The codeposition of nanocrystalline Au/B_4C composites has been investigated by Bicelli [30]. Considerable stabilization of nanosize under prolonged heat treatment can be obtained by dispersion of ceramic particles within the nanocrystalline matrix. Hardness values typical of nanometric systems can be preserved even after prolonged heat treatment in composite systems. Instrumented indentation measurements have been used for evaluation of hardness, Young's modulus, and plasticity of freestanding nanocrystalline metal and composite foils. The wear behavior of nanodeposited Au and composites has been evaluated by the pin-on-disk technique.

Au-Cu

Bossini et al. [31] developed baths based on $Au(CN)2^-$, Cu(I)-CN^-, Cu(II)-EDTA, and Cu(II) for the electrodeposition of equiatomic alloys. The effects of the dispersion of ceramic particles on structure evolution kinetics have been investigated. In another work, Bossinin et al. [32] investigated the hydrogen-related nanometric voids and their annealing behavior using thermal desorption spectroscopy and SAXS. The effects of the nature of chelating agents on geminate density were studied by XRD peak analysis. Tensile test results showed the mechanical effects connected to the use of different Cu(II) chelating agents, which can be explained with different densities of hydrogen-related nanovoids present in the electroformed alloys.

Co-Based Alloys

According to Bartlett et al. [27] and Herrasti et al. [28], nanocrystalline cobalt and cobalt-based are good candidates for the replacement of the highly toxic hexavalent chromium in electroplating baths, due to their excellent mechanical and wear-resistant properties. These materials have high saturation magnetization and good thermal stability. Improving hardness levels for nanocrystalline cobalt and its alloys over the polycrystalline counterparts has been reported. Electrochemically prepared Co nanodeposits have three to five times higher coercivity (Hc) than conventional polycrystalline Co.

Co-Fe

Koay et al. [33] have studied the magnetic properties, such as M_s and H_c, of Co-Fe alloys based on their different alloy compositions in electrolytes. It was found that the values of M_s and H_c increased linearly with additional contents of Fe. The increase in the M_s value was correlated to the crystal structure or phases of the films. The coexistence of both Co-Fe face-centered cubic (FCC) was confirmed.

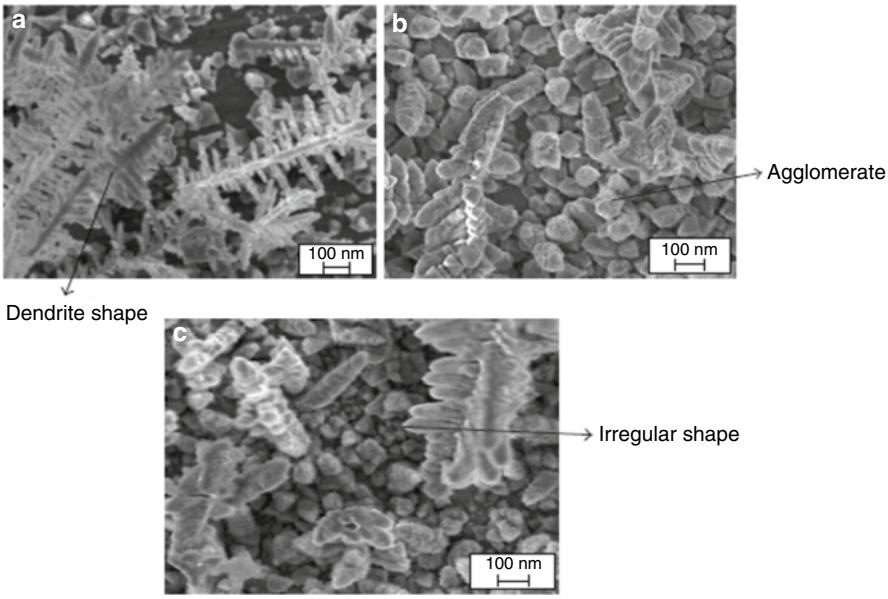

Fig. 4 FESEM micrographs of Co-Fe nanocoatings as a function of deposition time: (**a**) 30, (**b**) 60, and (**c**) 90 min [33]

Additionally, initial research works reported that, for nanocrystalline materials, there was a large reduction in M_s with finer grain size formation. It was stated that 40 % decrease in M_s for nanocrystalline Fe compared to its bulk polycrystalline was confirmed. Figure 4 illustrates the dendritic microstructure of Fe-Co nanodeposits, as a function of deposition time [33].

Co-Ni-Cu

Wang et al. [34] studied the electrodeposition of Co-Ni-Cu ternary nanodeposit using a mixture of $CoCl_2$, $NiCl_2$, and $CuCl_2$. Three-dimensional CoNiCu nanonetwork structure exhibited good performance as a catalyst for hydrogen evolution reaction (HER). Figure 5 shows the dendritic microstructure of such deposits.

Co-Ni-P

Ternary Co-Ni-P nanodeposits were successfully prepared by electrodeposition using a chloride bath containing boric acid and NaH_2PO_2. The morphology of the obtained layer was dependent on the concentration of Hypophosphite. As the concentration of Hypophosphite was increased, smooth deposits successively changed to dendritic, nodular, and again smooth. The crystalline structure can be either fcc or hcp, according to the dominating Fe-group metal content. The preferred orientation varies in a complex way with the bath and alloy composition. The deposition conditions have limited effects on the grain size of the alloys (ca. 50 nm). The magnetic properties are mainly dependent on the amount of codeposited P [35].

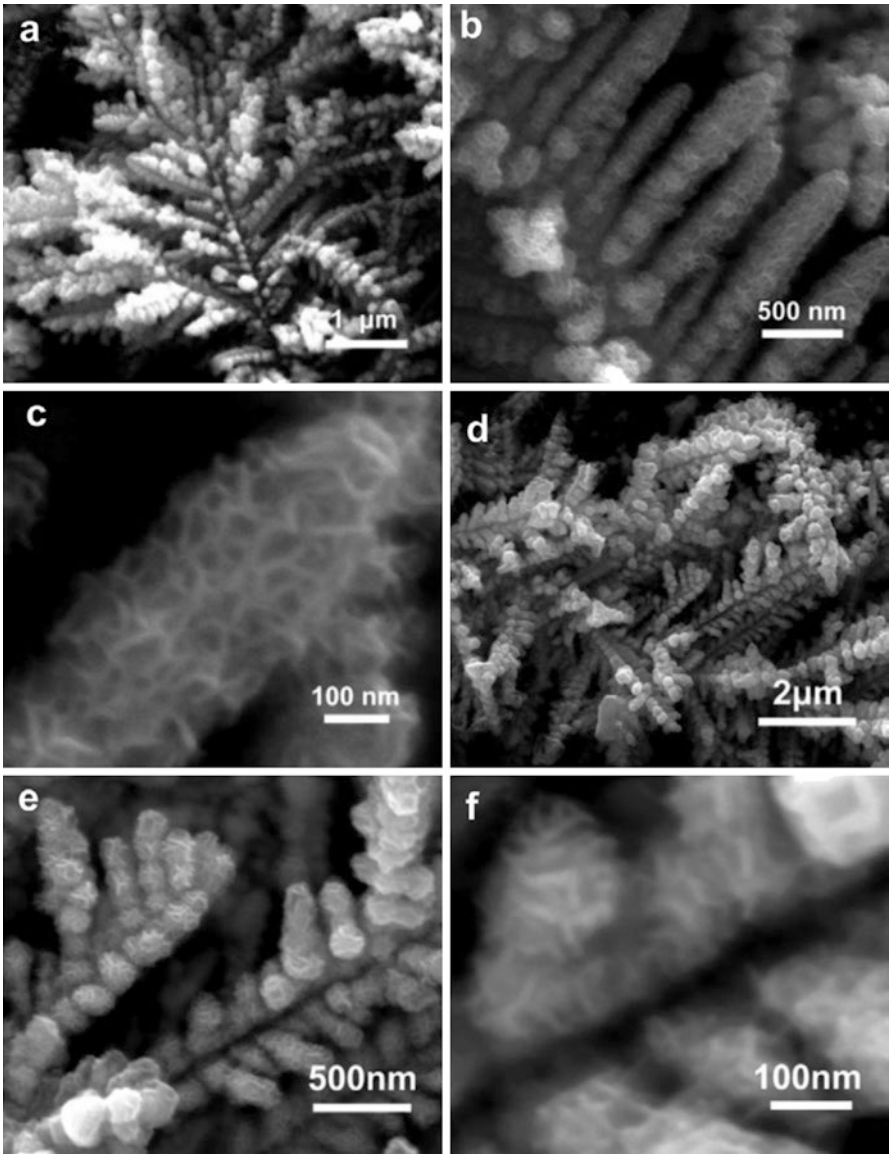

Fig. 5 SEM of the as-deposited dendritic-like morphology of CoNiCu alloy deposited in a mixed solution with 0.02 mol/L $CoCl_2$, 0.02 mol/L $NiCl_2$ and 0.01 mol/L $CuCl_2$ for 15 min [34]

Copper-Based Deposits

Coarse-grain copper is widely used in electrical and electronic devices despite the fact that it readily corrodes in a variety of environments [28]. Delplancke et al. [36] studied the electrodeposition of bimodal nanograined structures, with simultaneous presence of coarse (500 nm) and n-metric (100 nm) copper grains [36]. Natter et al. [37] reported significant tensile strength of copper nanodeposits due to small grain size and high defect density. The nature and concentration of organics added to the electrodeposition bath affecting the nanograin dimensions. Bicelli et al. [30] stated that room-temperature recrystallization behavior has a significant bearing on the stability of the electrical quantities of electronic devices implementing electrodeposited Cu, which tends to exhibit time-dependent properties. Annealing at moderate temperature is therefore common practice to avoid uncontrolled aging of these materials. The development of a <100> texture under low-temperature annealing has been reported. Ebrahimi et al. [38] stated that the annealing of 100 nm grain copper deposits up to 423 K displayed a limited (ca. 20 %) grain growth and no measurable variation of yield strength; concomitantly, a notable improvement of ductility and ultimate tensile strength was observed. Hall–Petch behavior of hardness was reported.

Cu-Fe

"Nanocrsytalline two-phase" Cu-Fe alloys (0–60 w% Cu) consisting of a mixture of fcc Cu {111} preferred orientation and bcc Fe {211} preferred orientation have been electrodeposited using sulfate-citrate bath. For the lowest content of Fe, the details of the evolution of the magnetic moment of the alloys were obtained by SQUID magnetometry. Increase of $CuSO_4$ concentration led to grain refinement [39].

Cu-Ni

Cu-Ni nanodeposits were obtained by pulse plating, and single-phase fcc alloys (26–36 w% Cu) with grain size in the range 2.5–28.5 nm and <111> texture have been obtained. Adjusting the pulse plating parameters can lead to formation of smooth, bright, and nodular surface morphology. Tensile stress layers galvanostatically deposited are higher in comparison with pulse-plated ones. The residual tensile macrostress of a range of Ni-Cu alloys was studied by spiral contractometry and the microstresses measured by the peak-broadening of XRD peaks [30]. Wolf et al. [40] stated that hyperfine interactions were detected due to a disordered grain boundary structure. The presence of Ni precipitates below the detectability limit of XRD was inferred from PAC measurements. Low current densities, higher temperatures, and addition of saccharin can improve the homogeneity of the NiCu alloy.

Nickel-Based Deposits

The electrochemical behavior of nickel and its oxides is important for applications such as rechargeable batteries, fuel cells, catalysis, and decorative coatings. Among various electrodeposited nanocrystalline metals, Ni-based alloys have been extensively researched due to their distinct properties such as being five times harder, reduction in coefficient of friction by 50 %, improved corrosion resistance, increased wear resistance by a factor of 170, improved electrocatalytic activities for hydrogen evolution and hydrogen oxidation reactions, and higher hydrogen diffusion [2]. Pure Ni film and eight Ni-based alloy films (Ni-W, Ni-P, Ni-Mo, Ni-Co, Ni-Cu, Ni-Zn, Ni-Mg, and Ni-B) were deposited and characterized. More systematic studies were conducted for Ni-W and Ni-P films, along with pure Ni film as a baseline [6].

NC nickel of about 17 nm size produced by ED significantly enhances the electrocatalytic activity for hydrogen evolution due to the increased density of active surface sites [41].

According to Rashidi et al. [6], at the current densities higher than 75 mA/cm^2, in the absence of saccharin the nickel layer exhibits a pyramidal-like morphology (Fig. 6a) while it changes to a colony-like morphology in presence of saccharin. An increase in current density results in larger colonies and brighter appearance (Fig. 6b, c).

Ni-W Alloys

Weston et al. [42] studied the properties of Ni-W nanodeposits. Ni-W alloy was introduced to replace chromium coatings because they are environmentally friendly. Ni-W alloys have various industrial applications because of their excellent material and physical properties. First, the deposited Ni films exhibit hardness of a range from 2 to 7 GPa, depending on the actual grain size. Second, these nanocrystalline Ni-W films exhibit excellent corrosion rates as low as ~2.5 % of that of a typical conventional stainless steel. Third, these Ni-W alloys would be used as diffusion barriers between copper and silicon in ultralarge-scale integration (ULSI) circuits and microelectromechanical systems (MEMS). Nickel–tungsten alloys with grain size of around 20 nm lead to low friction and wear, and the hardness of nickel–tungsten electrodeposits increases significantly as the crystallite size is reduced from around 50 to 10 nm.

The W dopants were introduced by adding a tungsten salt into nickel sulfate ($NiSO_4$) to form Ni-W alloys; interestingly, it is rather difficult to deposit pure W films without depositing Ni simultaneously. Usually, ammonium chloride (NH_4Cl) and/or citric acid (Cit) are also added into the deposition bath to improve Faradaic efficiency (FE), to control the pH value, and to increase solubility of metal ions.

A characteristic relationship between composition and grain size has been illustrated, which is explained from the W segregation that reduces the grain boundary energy as the driving force for grain growth. Some studies stated that when tungsten atomic percentage is increased from 2.5 % to 23 %, the corresponding grain size is

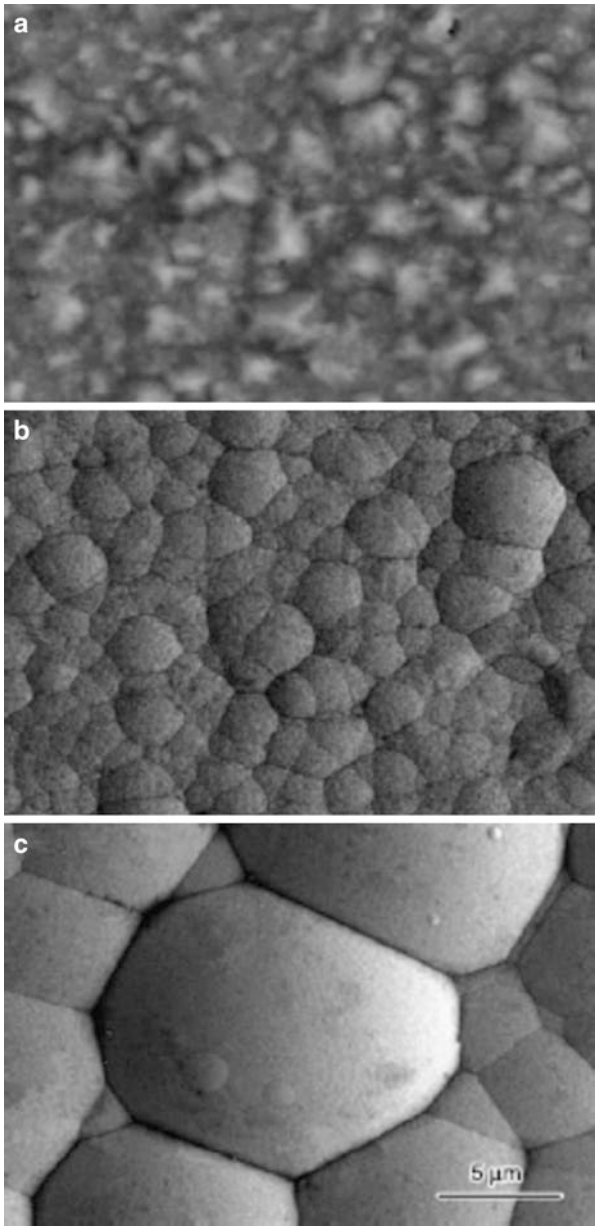

Fig. 6 SEM micrographs of nickel coatings deposited as a function of working parameters: (**a**) saccharin-free bath at $i = 100$ mA/cm^2, (Pyramidal-like) (**b**) bath containing 5 g/L saccharin at $i = 100$ mA/cm^2, (colony-like) (**c**) bath containing 5 g/L saccharin at $i = 300$ mA/cm^2 (large colony-like) [6]

decreased from >100 to <10 nm. In addition to XRD peak broadening that is associated with reducing grain size, shifts in XRD peak position were also observed. This is because the solution of larger tungsten atoms increases the lattice parameter of the FCC alloys [43].

Ni-Co Alloys

Alloys of iron group metals, Fe, Co, and Ni, have been considered as very good magnetic materials. These alloys are known to possess much better permanent magnetic properties than pure metals. Ni–Co alloys have been investigated as important engineering materials for several decades because of their unique properties, such as high strength, good wear resistance, heat conductivity, and electrocatalytic activity. Electrodeposited Ni–Co thin films have been intensively studied due to their application in MEMS. Thin and thick Ni–Co films form important parts of magnetic-MEMS devices including sensors, microactuators, or micromotors because of their excellent physical properties. Fine Ni, Co, and Ni–Co alloy powders are required for developing magnetoresistive sensors in thick-film form [44].

Liping et al. [45] showed that Co content affects the morphology and grain size of alloys. The phase structure of Ni–Co alloys gradually changed from fcc to hcp structure with the increase of Co content. The hardness of Ni–Co alloys with a maximum around 49 wt% Co followed the Hall–Petch effect. It was found that the improvement of wear resistance of Ni-rich alloys with hardness increase followed Archard's law. In addition, the Co-rich alloys exhibited much lower friction coefficient and higher wear resistance than Ni-rich alloys. It has been concluded that hcp crystal structure in Co-rich alloys contributed to the remarkable friction–reduction effect and better antiwear performance under the dry sliding wear conditions. According to Rafailovie [46], the structure morphology was converted from platelet to cauliflower structure by increasing Ni^{2+}/Co^{2+} ratio.

Ni-P Alloys

Ni–P deposits obtained from electrodepsoition are good catalysts for hydrogen evolution, special paramagnetic properties, excellent microhardness, and corrosion resistance [47]. Ni-P alloys have been studied to a less extent than Ni-W alloys. Nevertheless, a similar relationship between the P content and resultant grain size has been reported. Like W, although it is feasible to add P dopants into the iron-group metals during electrodeposition, deposition of P alone is difficult [48]. Two possible deposition mechanisms were suggested for electrodeposition by Erb et al. [49]. The "direct" deposition mechanism assumes that the phosphorus element forms from the reduction of phosphorus oxyacid in the aqueous solutions;

$$Ni^{2+} + 2e^{-} \rightarrow Ni_{ad}H \tag{6}$$

$$2PHO_3 + 3H^{+} + 3e^{-} \rightarrow P_{ad} + 3H_{2n}NiO_{ad} + P_{ad} \rightarrow N_{in} \tag{7}$$

However, this mechanism is not convincing, because direct deposition of pure elemental phosphorus is not possible. Alternatively, the "indirect" deposition mechanism assumes that the reduced phosphine from phosphorus oxyacid reacts with $Ni^{2+}H$ in the bath and produces Ni-P alloys, i.e.,

$$2PHO_3 + 6H^{+} + 6e^{-} \rightarrow PH_3 + 3H_2 \tag{8}$$

$$PHO_3 + 3Ni^{2+} \rightarrow 2P + 3Ni + 6H^{+} \tag{9}$$

Nanocrystalline Ni-P alloys and coatings have excellent corrosion resistance, electrochemical catalytic properties [50], and nonmagnetic character [51]. Amorphous Ni-P coatings that contain more than 10 at.% P were found to be highly effective for corrosion resistance [52]. In addition, Ni-P alloys are used in MEMS devices and electronics.

Ni-Mo Alloys

According to Schulz et al. [53], the enhanced HER kinetics of Ni-nanodeposits are due to the high area fraction of grain boundaries (and to some extent, triple junctions) intersecting the free surface of the electrode. The HER kinetics can be further enhanced by alloying nanocrystalline Ni with molybdenum. Ni-Mo deposits are good catalysts for hydrogen production from water by electrolysis as well as by steam reforming of hydrocarbons. Halim et al. [54] prepared nodular Ni-Mo nanocrystalline deposits (Fig. 7) by galvanostatic electrodeposition from citrate-ammonia solutions. According to XRD analysis, a single Ni-Mo solid solution phase was detected. The size of the nodules increased as electroplating current density increased. From EDX analysis, as the current density increased from 5 to 80 $mA \cdot cm^{-2}$, the molybdenum content in the deposits decreased from ~31 to 11 wt%. Nanolayers with 23 % Mo exhibited the highest microhardness value (285 Hv). Mo content values between 11 % and 15 % are recommended for obtaining high corrosion resistance and better electrocatalytic activity for HER.

Nickel-based composite coatings are characterized by their high catalytic activity for hydrogen evolution (HER) and electrocatalytic oxygen evolution (OER) as well as good corrosion resistance in aggressive environments. Ni–Mo nanocomposite layers (18–32 nm) were prepared by galvanostatic electrodeposition from a nickel salt bath containing suspended Mo nanoparticles. According to XRD analysis, the nanodeposits consisted of crystalline Mo incorporated into Ni matrix. The molybdenum content decreased by increasing the deposition current density and ranged between ~6 % and ~17 % Mo. The crystallite size and the surface roughness increased by increasing the current density (Fig. 8). The corrosion rate of Ni–Mo composites increased with increasing Mo content due to crystallite size-refining and surface roughness effect. Electrocatalytic effect for hydrogen production was improved mainly due to higher surface roughness and thus providing more accessible surface area [55].

Template–Assisted Electrodepostion

Nanowires and nanorods of defined dimension were successfully prepared using templated synthesis. Several techniques of forming nanomaterials using templates have been developed such as chemical vapor deposition (CVD), sol–gel deposition, polymerization, and electrochemical deposition. The template-assisted electrodeposition has been successfully used to prepare 1D nanostructures of various metals, semiconductors, and conductive polymers. Template synthesis in nanoporous membranes have been carried out in anodic aluminum oxide, polycarbonate, and diblock copolymer membranes [56, 57].

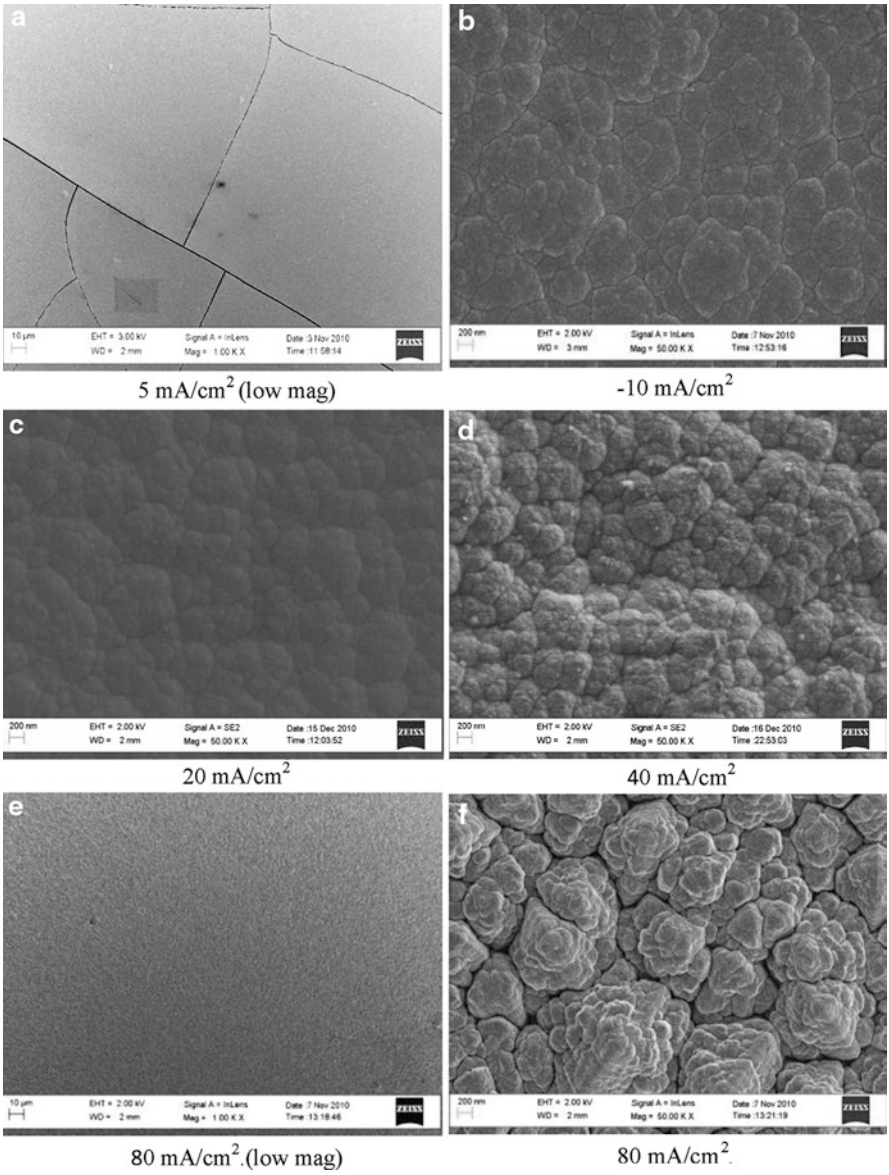

Fig. 7 SEM micrographs of Ni-Mo nanodeposits showing nodular shaped microstructure [54]

Conclusions

Electrodeposition has been identified to be a technologically feasible and economically superior technique for the production of nanocrystalline pure metals and alloys as well as nanocomposites. Electrodeposition of polycrystalline metals and alloys exhibits several types of growth forms including layers, blocks, ridges, dendrites,

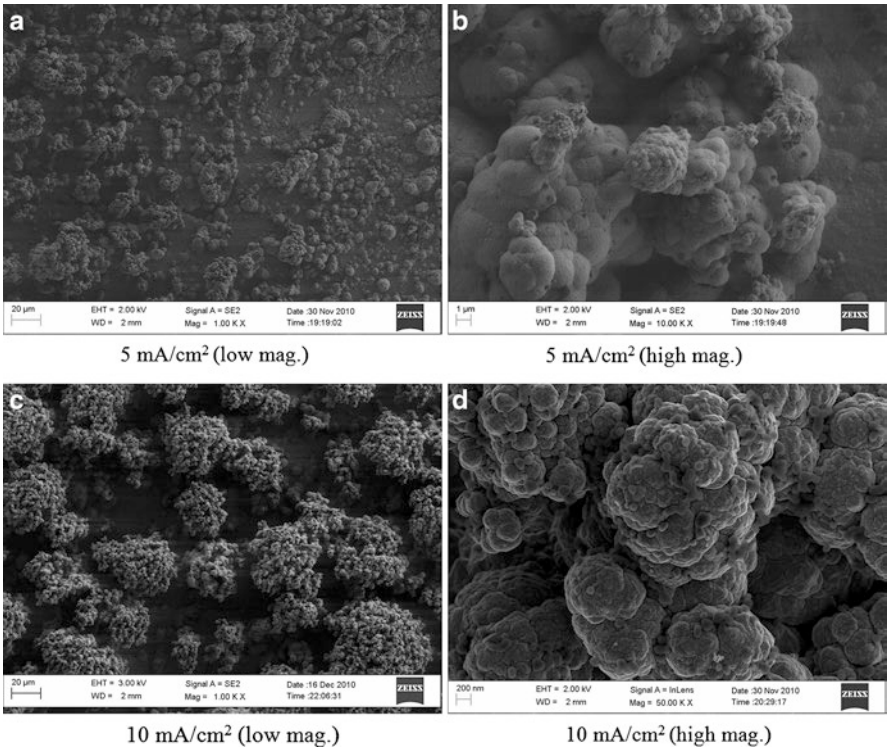

Fig. 8 SEM micrographs for electrodeposited Ni-Mo Nanocomposites showing clusters formation [55]

pyramids, spiral growth forms, powders, and whiskers. Research on the structure–property-performance relationships of these materials has indicated many promising properties which can be exploited for commercial purposes. Of all the nanoprocessing techniques, electrodeposition appears to be a promising technique due to its relatively low cost, ability to produce compositions unattainable by other techniques, and the possibility of forming of simple low-cost multilayers in many different systems. Consequently, new markets and business opportunities are expected to emerge for the electroplating industry.

References

1. Gleiter H (1981) Deformation of polycrystals: mechanisms and microstructures. In: Hansen N, Horsewell A, Liholt H (eds) Proceedings of the 2nd Riso international symposium on metallurgy and materials science. Riso National Laboratory, Roskilde, p 15
2. Rofagha R, Wood D, Erb U (1993) Industrial applications of nanocrystalline electrodeposits. In: Yacaman MJ, Tsakalakos T, Kear BH (eds) Proceedings of the first international conference on nanostructured materials, Cancun. Nanostructured materials, vol 3. pp 1–6
3. Gurrappa I, Binder L (2008) Electrodeposition of nanostructured coatings and their characterization – a review. Sci Technol Adv Mater 9:043001 (11 pp)

4. Bockris JOM (1964) Modern aspects of electrochemistry, vol 3. Butterworths, London, p 224
5. Mohanty US (2011) Electrodeposition: a versatile and inexpensive tool for the synthesis of nanoparticles, nanorods, nanowires, and nanoclusters of metals. J Appl Electrochem 41:257–270
6. Rashidi AM, Amadeh A (2010) Effect of electroplating parameters on microstructure of nanocrystalline nickel coatings. J Mater Sci Technol 26(1):82–86
7. Bakonyi I, Toth-Kadar E, Toth J, Tarnoczi T, Cziraki A (1996) In: Suryanarayana C (ed) Processing and properties of nanocrystalline materials. TMS, Warrendale, PA, pp 465–471
8. McMahon G, Erb U (1989) Structural transitions in electroplated Ni-P alloys. Microstruct Sci 17:447–455
9. Abdel-Karim R, Reda Y, Muhammed M, El-Raghy S, Shoeib M, Ahmed H (2011) Electrodeposition and characterization of nanocrytalline Ni-Fe alloys. J Nanomater 2011:519274
10. Alfantazi AM, El-Sherik AM, Erb U (1994) The role of nickel in the morphology evolution of pulse plated Zn-Ni alloy coatings. Scr Metall Mater 30(10):1245–1250
11. Osmola D, Renaud E, Erb U, Wong L, Palumbo G, Aust KT (1993) Synthesis of nanocrynalline Co-W alloys. Mater Res Soc Symp Proc 286:191–196
12. Cheung C, Erb U, Palumbo G (1994) Application of grain boundary engineering concepts to alleviate stress corrosion cracking in alloys 600 and 690. Mater Sci Eng 185A:39–43
13. El-Raghy SM, Abdel-Karim R, Khalaf A, Ayman K, Aziz L (2012) Surface characterization and corrosion properties of nanocrystalline Ni-based coatings. In: International conference on corrosion mitigation and surface protection technologies, Hurghada, 10–13 Dec
14. Boukherroub R, Szunerits S (2009) Wet chemical approaches for chemical functionalization of semiconductor nanostructures. In Schmuki P, Virtanen S (eds) Electrochemistry at the nanoscale. New York: Springer, chapter 5
15. Albert Calbetó S (2011) Nickel matrix micro/nano SiC composite electrodeposition. Escola Tècnica Superiord'Enginyeria Industrial de Barcelona, Master thesis, Spain
16. Khalaf A, Ayman K, Aziz L (2012) Electrodeposition and characterization of nanocrystalline Ni-based deposits. BSc Graduation Project, Department of Metallurgy, Cairo University
17. Kanani N (2004) Electroplating – basic principles, processes and practice. Elsevier, Amsterdam
18. Winand R (1994) Electrodeposition of metals and alloys-new results and perspectives. Electrochem Acta 39(8/9):1091–1105
19. Watanabe T (2004) Nano-plating- microstructure control, theory of plated film and data base of plated film microstructure. Elsevier, Amsterdam, chapter 2
20. Venables J (2000) Introduction to surface and thin film processes. Cambridge University Press, Cambridge
21. Oura K, Lifshits VG, Saranin AA, Zotov AV, Katayama M (2003) Surface science: an introduction. Springer, Berlin
22. Pimpinelli AO, Villain J (1998) Physics of crystal growth. Cambridge University Press, Cambridge
23. Markov IV (1995) Crystal growth for beginners: fundamentals of nucleation, crystal growth, and epitaxy. World Scientific, Singapore
24. Matthews JW (1975) Epitaxial growth. Academic, New York
25. Fischer H (1954) Elektrolytlsche Abscherdung und Elektroknstalbsatzon von Metallen Berhn. Springer, Berlin, p 729
26. Elias J, Gizowska M, Brodard P, Widmer R, deHazan Y, Graule T, Michler J, Philippe L (2012) Electrodeposition of gold thin films with controlled morphologies and their applications in electrocatalysis and SERS. Nanotechnology 23:255705 (7 pp)
27. Bartlett PN, Birkin PN, Ghanem MA, Groot P, Sawicki M (2001) The electrochemical deposition of nanostructured cobalt films from lyotropic liquid crystalline media. J Electrochem Soc 148:C119–C123
28. Herrasti P, Ponce de León C, Walsh FC (2012) The corrosion behavior of nanograined metals and alloys. Rev Metal 48(5):377–394
29. Bozzini B, Fanigliulo A, Serra M (2001) Electrodeposition of star-shaped gold crystallites. J Cryst Growth 231:589–598

30. Bicelli LP, Bozzini B, Mele C, D'Urzo L (2008) A review of nanostructural aspects of metal electrodeposition. Int J Electrochem Sci 3:356–408
31. Bozzini B, Giovannelli G, Cavallotti PL (2000) Part II – baths not containing free cyanide. J Appl Electrochem 30:591–594
32. Bozzini B, Giovannelli G, Natali S (2000) Metastable structures in electrodeposited AuCu. Scr Mater 43:877–880
33. Koay MH, Wan Normimi RA, Azrina Resali N, Chong WT, Salleh Z, Ghani MA (2013) The physical and magnetic properties of electrodeposited Co-Fe nanocoating with different deposition times. J Nanomater 2013, Article ID 680491, (6 pp)
34. Wang C, Li W, Lu X, Xie S, Xiao F, Liu P, Tong Y (2012) Facile synthesis of porous 3D CoNiCu nano-network structure and their activity towards hydrogen evolution reaction. Int J Hydrog Energy 37:18688–18693
35. Park D-Y, Myung NV, Schwartz M, Nobe K (2002) Electrodeposited CoNiP films. Electrochim Acta 47:2893–2900
36. Delplancke JL, Sun M, O'Keefe TJ, Winand R (1989) Nucleation of electrodeposited copper on anodized titanium. Hydrometallurgy 23:47–66
37. Natter H, Hempelmann R (1996) Nanocrystalline copper by pulsed electrodeposition. J Phys Chem 100:19525–19532
38. Ebrahimi F, Zhai Q, Kong D (1998) Mechanical properties of Cu/Ag multilayered composition. Mater Sci Eng A 255:20–32
39. Williams JM, Blythe HJ, Fedosyuk VM (1996) An investigation of electrodeposited granular Cu Fe alloyed films. J Magn Magn Mater 155:355–357
40. Wolf H, Guan Z, Li X, Wichert TH (2001) Magnetic properties of grain boundaries of nanocrystalline Ni and of Ni precipitates in nanocrystalline NiCu alloys. Hyperfine Interact 136/137:281–287
41. Haseeb A, Blanpain B, Wouters G, Celis JP, Roos JR (1993) Electrochemical deposition: a method for the production of artificially structured materials. Mater Sci Eng A 168:137–140
42. Weston DP, Shipway PH, Harris SJ, Cheng MK (2009) Friction and sliding wear behavior of electrodeposited cobalt and cobalt–tungsten alloy coatings for replacement of electrodeposited chromium. Wear 267:934–943
43. Park H (2008) Electrodeposition of nanocrystalline Ni-based alloys. Master thesis, Clemson University
44. Lidija D, Dragica R, Mninic M (2009) Deposition and characterization of nanostructured nickel-cobalt alloys. Hem Ind 63(5a):557–569
45. Liping W, Yan G, Qunji X, Huiwen L, Tao X (2005) Microstructure and tribological properties of electrodeposited Ni–Co alloy deposits. Appl Surf Sci 242:326–332
46. Rafailovic LD, Maricic AM, Artner W, Nauer GE, Minic DM (2009) Morphology and microstructure of annealed Ni-Co alloy powders electrodeposited on copper substrates. Sci Sinter 41:135–142
47. Daly BP, Barry F (2003) Electrochemical nickel-phosphorous alloy formation. J Int Mater Rev 48:326–338
48. Doyle DM, Palumbo G, El-Sherik AM, Erb U, Aust KT (1992) Proceedings of the nanophases nanocrystalline structure, California, Mar 1992, p 51
49. Erb U, Aust KT, Palumbo G (2002) Nanostructured materials processing, properties and technologies. William Andrew Publishing, Norwich, p 179
50. Siegel RW, Thomas GJ (1992) Grain boundaries in nanophase materials. Ultramiscroscopy 40:376–384
51. Ciubotariu AC, Benea L, Varsanyi ML, Dragan V (2008) Electrochemical impedance spectroscopy and corrosion behavior of Al2O3-Ni nano composite coatings. Electrochim Acta 53:4557–4563
52. Brooks I, Erb U (2001) Hardness of electrodeposited microcrystalline and nanocrystalline gamma-phase Zn-Ni alloys. Scr Mater 44:853–858
53. Schulz R, Huot J, Trudeau M (1994) Nanocrystalline Ni-Mo alloys and their application in electro catalysis. J Mater Sci 9:2998–3008

54. Halim J, Abdel-Karim R, El-Raghy S, Nabil M, Waheed A (2012) Electrodeposition and characterization of nanocrystalline Ni-Mo. J Nanomater 2012:845673, 10 pp
55. Abdel-Karim R, Halim J, El-Raghy S, Nabil M, Waheed A (2012) Surface morphology and electrochemical characterization of electrodeposited Ni–Mo nanocomposites as cathodes for hydrogen evolution. J Alloys Compd 530:85–90
56. Guangwei S, Lixuan M, Wensheng S (2009) Electrodeposition of one-dimensional nanostructures. Recent Pat Nanotechnol 3:182–191
57. Liu GQ, Zhao XS (2004) Nanoporous materials – science and engineering, vol 4, Series on chemical engineering. Imperial College Press, London, chapter 1